WILEY | Hindawi

Research Article

Experimental Investigation of the Seepage-Induced Failure Process in Granular Soils

Yu Wang [ID],[1] Xiangbao Duan,[2] Yanchang Gu,[2] and Shijun Wang[2]

[1]*College of Architectural Engineering, Jiangsu Open University, No. 399, The North Road of Jiangdong, Nanjing, Jiangsu, China*
[2]*Nanjing Hydraulic Research Institute, No. 223, Guangzhou Road, Nanjing, Jiangsu, China*

Correspondence should be addressed to Yu Wang; wangyu@jsou.edu.cn

Seepage-induced failure may disable the bearing capacity of foundations in dams and embankments. However, the evolution mechanism of the seepage failure process in granular soils is not well understood. In this paper, a series of laboratory hydraulic tests were performed to investigate the seepage failure process in sandy gravels and fine-grained sands. Seepage behaviors of the hydraulic gradient, seepage flow velocity, and permeability coefficient were observed, and then, the Reynolds number was obtained to describe the seepage regime. By linking the hydraulic gradients with the Reynolds number, the seepage failure process was quantitatively divided into four phases: (i) incubation (Re < 0.85), (ii) formation ($0.85 \leq Re \leq 5$), (iii) evolution ($5 < Re \leq 50$), and (iv) destruction ($50 < Re$). The findings of the study identified an approximately linear relationship between the hydraulic gradient and the seepage velocity in the phases of incubation and formation in which the viscous drag effects are not negligible, corroborating Darcy's view. However, in the phases of evolution and destruction, the hydraulic gradient and the seepage velocity are nonlinearly related, indicating that the inertial force plays a leading role, and the quadratic equation is relevant for the regime transition from laminar flow to turbulent flow. Finally, the mechanism of each phase in the seepage failure process was clarified. Fine content and uniformity coefficient are internal factors that affect the potential of seepage failure, while the seepage force that drives the transport of fine particles is an underlying cause that promotes the development of seepage failure. This study will be quite useful in identifying the limits of applicability of the well-known "Darcy's law," in further improving the physical modelling associated with fluid flow through granular soils.

1. Introduction

Dam safety is related to people's lives and property, flood defence, water supply, ecological conservation, and food production, which are vital to the national economy and society. However, in recent years, there have been some defects in engineering design, construction management, and regular maintenance, which have brought new potential safety hazards, such as sinkholes in roads, the collapse of foundation pits, and the breaching of dams [1–3]. For example, the February 2017 failure of the spillway chute at Oroville Dam, owned and managed by the California Department of Water Resources (DWR), raises great concerns for joints and fractures of concrete spillway chutes that could allow high-pressure water to penetrate a chute foundation [4]. Investigations have shown that seepage-induced failure of granular soils in the foundation is the most important cause of chute slab failure under high-velocity flow conditions. Beyond that, it is reported that seepage failure (i.e., piping, heave, and leakage) accounts for nearly half of the dam and levee breaking accidents all over the world [5–8]. Given the risk of seepage failure in granular soils, it is essential to clarify the evolution mechanism of the seepage failure process to ensure the long-term safety of project operations.

Seepage failure takes the following forms in the initiation and evolution process: suffusion, backward erosion, concentrated leak, and contact erosion [9]. Suffusion describes the process by which the finer particles move through the voids of the coarser particles without any change in the total volume [10]. Backward erosion indicates that the surface particles are detached from the downstream exit and gradually develop along the seepage flow direction [11]. Concentrated

leak mostly takes place in cohesive soil with the seepage path like a crack [12]. Contact erosion refers to the phenomenon that the fine soil is eroded by seepage flow through the interface between the coarse soil and the fine soil [13, 14]. Despite the various types of seepage failure, research has identified that seepage failure stems from soil particle migration along the seepage flow path [15]. As seepage erosion develops progressively in granular soils, hydromechanical characteristics are altered, resulting in an increase in permeability and instability of structures [16].

Nevertheless, due to the diversity of the soil structure and the complexity of the fluid regime, it is difficult to clarify the hydromechanical characteristics of the entire seepage failure process. Henry Darcy, in an appendix of his work *Les Fontaines Publiques de la Ville de Dijon*, proposed the law governing the seepage flow through a saturated, isotropic, and uniform sand filter [17]. In Darcy's law, the superficial flow velocity is linearly correlated to hydraulic gradient, i.e.,

$$\frac{\Delta p}{L} = \frac{\mu}{k_d} v, \tag{1}$$

where p is the fluid pressure, L is the length between the inlet and outlet, k_d is the Darcy permeability, μ is the fluid viscosity, and v is the flow velocity. Darcy flow has been widely used to simulate groundwater flow ever since. Generally, Darcy flow can be divided into prelinear flow and postlinear flow. Prelinear flow at low velocity takes place in fine-grained particles due to the electrochemical surface effect between the solid particles and the fluid, while postlinear flow at high velocity is often observed in fractured or coarse-grained media because of the inertial effect and the onset of turbulent flow [18]. However, it may no longer follow Darcy's law because the flow velocity of seepage is either high or low. Furthermore, numerous project practices have demonstrated that Darcy's law holds only for a low Reynolds number (creeping flow regime) but not for a higher Reynolds number [19]. The Reynolds number is the nondimensional parameter to describe the fluid regime as follows:

$$\text{Re} = \rho \frac{vd}{\mu}, \tag{2}$$

where Re is the Reynolds number, ρ is the fluid density, v is the flow velocity, μ is the fluid viscosity, and d is the characteristic length, generally expressed by d_{50} for the mean grain size [20]. In terms of the seepage failure, the linear proportion of hydraulic gradient to seepage flow velocity (J-v curve) transforms when the hydraulic gradient reached the critical value. Subsequently, it presents unsteady, nonlinear, and high flow characteristics as the fine particles gradually transport from the soils, which deviates from Darcy's law [18, 21]. One of the nonlinear formulations in the non-Darcy regime is the Forchheimer equation [22], which adds

a quadratic term of flow velocity into Darcy's law as follows:

$$\frac{\Delta p}{L} = \frac{\mu}{k_f} v + \beta \rho v^2, \tag{3}$$

where k_f is the Forchheimer permeability, β is the non-Darcy coefficient, and ρ is the fluid density. Another nonlinear formulation in the non-Darcy regime is the Izbash exponential equation as follows [17, 23]:

$$\frac{\Delta p}{L} = av^m, \tag{4}$$

where a is the constant and m represents the variable parameter subjected to fluid regime change (i.e., if the seepage flow regime is laminar, then $m = 1$; if the seepage flow regime is turbulent, then $m = 2$; and if between laminar and turbulent flow, then $m = 1 \sim 2$). Previous research results have verified the robustness of such two equations in describing non-Darcy flow [24–28]. However, none of them yielded a "universal" correlation due to the complexity of the soil structure and fluid regime [29–32].

Previous studies have mainly focused on the different types of seepage failures and critical hydraulic gradients, while the fluid regime changes caused by seepage failures deserve more attention. In addition, various mechanisms of the seepage failure process have been identified, but every phase of the seepage failure process has not been qualitatively recognized or discriminated. Therefore, it is difficult to scientifically judge the potential and predict the development of seepage failure. The primary objective of this study is (i) to evaluate the hydraulic conditions initiating seepage failure in sandy gravels and fine-grained sands, (ii) to obtain the Reynolds number required for regime change on the basis of hydraulic conditions, and (iii) to provide a novel quantitative description method of the distinction of each phase in the seepage failure process. Specifically, this paper presents a series of laboratory tests to show seepage behaviors of hydraulic gradient, seepage flow velocity, and permeability coefficient. Then, the description method of each phase of the seepage failure process was quantitatively proposed by the Reynolds number, allowing it to describe the seepage flow regime change with the removal of fine particles. The results will not only provide more knowledge about the evolution mechanism of the seepage failure process but also provide an important reference for the prevention of seepage failure in practice.

2. Materials and Methods

2.1. Testing Soils. Tests were performed on granular soil from the banks of the Yangtze River, including five samples of natural sandy gravels numbered A~E (Figure 1), four samples of natural fine-grained sands numbered F~I (Figure 2), and four samples of laboratory-made sandy gravels numbered 1~4 (Figure 3). Different parameters of natural soils were compared with those of laboratory-made soils in the initial seepage failure process. Specifically, natural soils with successive grading were prepared for seepage
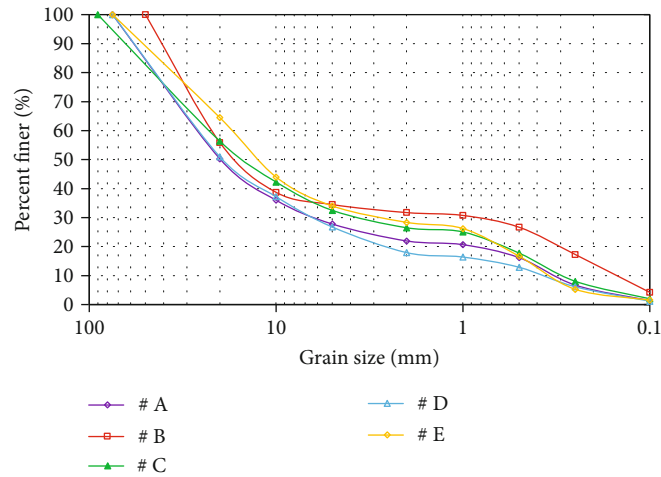
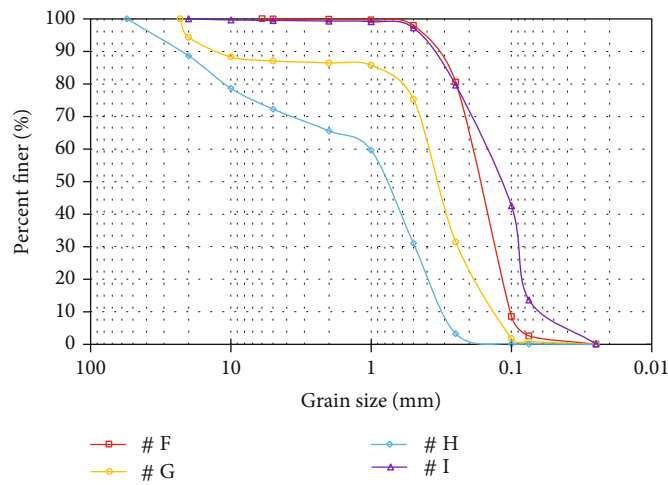FIGURE 1: Grading curve of natural sandy gravels numbered A~E.

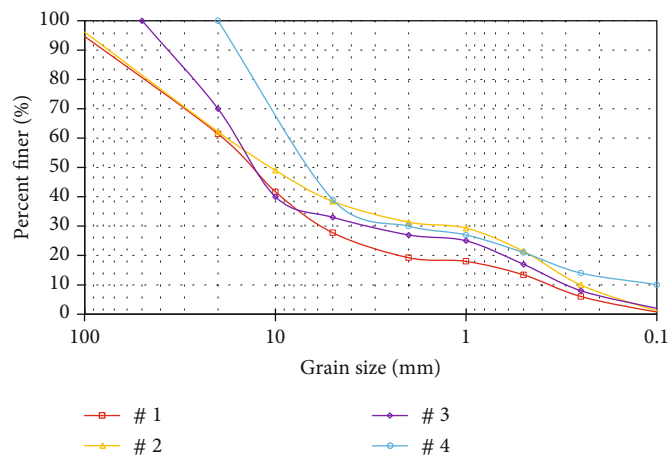FIGURE 2: Grading curve of natural fine-grained sands numbered F~I.

FIGURE 3: Grading curve of laboratory-made sandy gravels numbered 1~4.

deformation tests to show hydraulic gradient changes by measuring water pressures, overflow amounts, and sand boiling amounts. Comparative tests of natural soils with laboratory-made soils that differ in fine particle content and uniformity were carried out to show soil structure changes in the seepage failure process. For particle flow tests,

TABLE 1: Physical parameters of different soil samples.

Soil number	Soil type	Uniformity coefficient C_u	d_{50} (mm)	Porosity n	Dry density ρ_d (g/cm^3)	Permeability K (cm/s)
A	Sandy gravel	81.25	20.00	0.26	1.96	$3.35E-02$
B	Sandy gravel	150.00	16.00	0.29	1.89	$3.20E-03$
C	Sandy gravel	73.30	14.00	0.22	2.08	$1.10E-02$
D	Sandy gravel	66.70	20.00	0.24	2.02	$1.02E-02$
E	Sandy gravel	45.70	11.00	0.27	1.94	$1.10E-02$
F	Fine-grained sand	1.80	0.15	0.46	1.43	$3.20E-03$
G	Fine-grained sand	3.33	0.77	0.32	1.80	$4.00E-02$
H	Fine-grained sand	2.10	0.11	0.47	1.40	$7.00E-04$
I	Fine-grained sand	3.33	0.32	0.38	1.65	$2.50E-02$
1	Sandy gravel	58.80	12.00	0.24	2.02	$3.35E-02$
2	Sandy gravel	78.30	10.00	0.22	2.07	$4.00E-03$
3	Sandy gravel	35.00	10.20	0.22	2.04	$2.39E-03$
4	Sandy gravel	80.50	7.00	0.27	1.93	$6.55E-03$

FIGURE 4: Schematic illustration of testing apparatus.

laboratory-made soils with gapped grading were also prepared to clarify the factors affecting the mechanisms of the seepage failure process.

Experimental soils were prepared as follows. For natural soil samples, the cutting edge was used to press vertically into soils until they were filled in the ring sampler; then, surrounding soils were cut off, and the ring sampler was carefully taken out to keep natural soils undisturbed. For laboratory-made soil samples, they were divided into 10 representative grades in the light of different aperture sifters, that is, >20 mm, 20 mm~10 mm, 10 mm~5 mm, 5 mm~2 mm, 2 mm~1 mm, 1 mm~0.5 mm, 0.5 mm~0.25 mm, 0.25 mm~0.1 mm, 0.1 mm~0.075 mm, and 0.075 mm~0.025 mm. Especially for large-size gravels (maximum grain diameter of 3 cm), an equivalent density method was used to keep the soil unit weight invariant by using fine particles instead of large ones. The physical parameters of different soil samples are presented in Table 1.

2.2. Testing Apparatus. A testing apparatus was used to measure the hydraulic gradients and seepage pressures under the conditions of vertical seepage flow through a soil sample (Figure 4). The general concept of the apparatus is to provide a uniform hydraulic gradient through a soil sample,
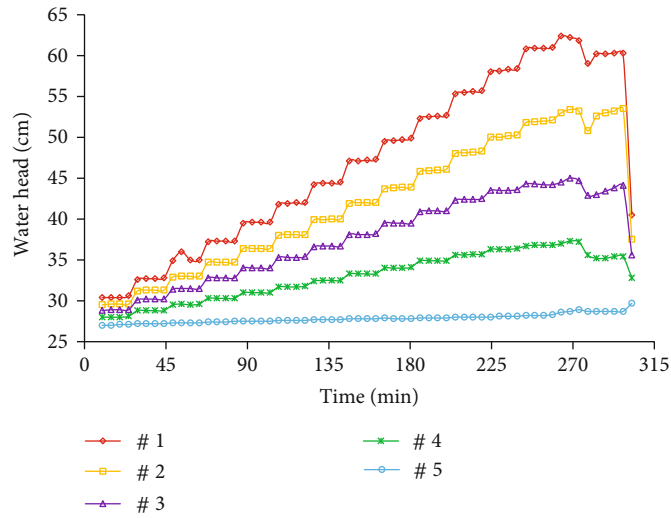
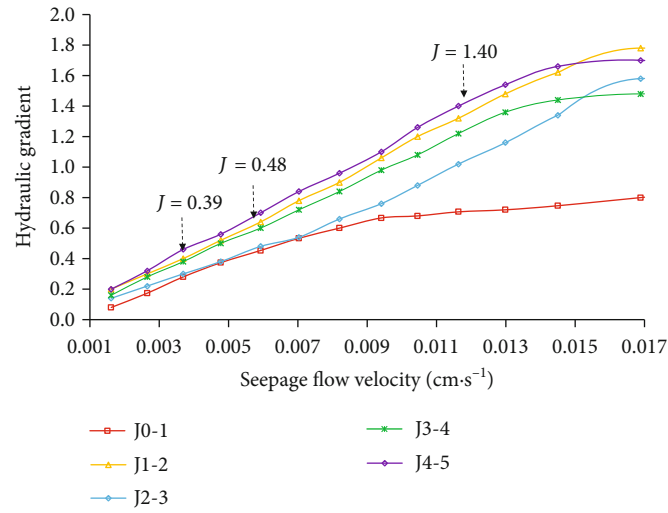Figure 5: Process curve of water head of different piezometers in soil numbered C.

Figure 6: Process curve between hydraulic gradient and seepage flow velocity of different parts in soil numbered C.
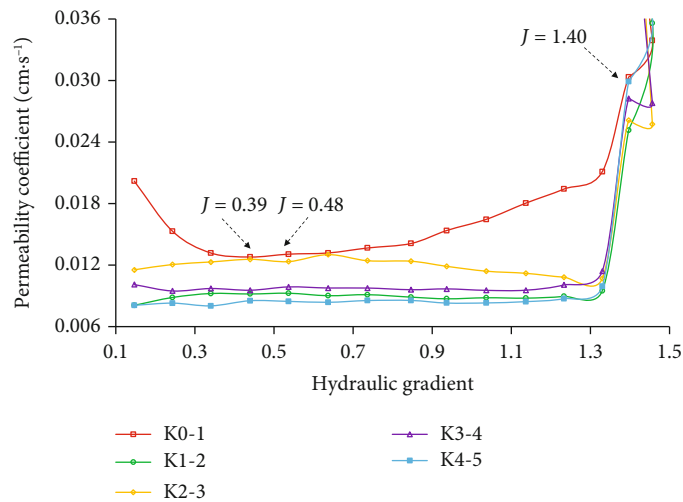
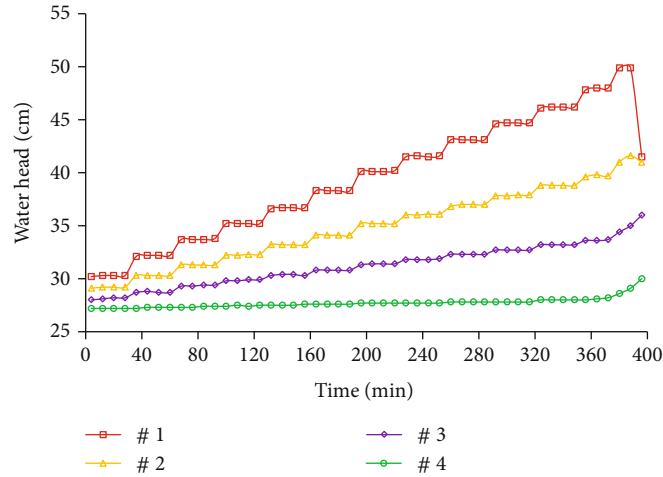Figure 7: Process curve between hydraulic gradient and permeability of different parts in soil numbered C.

Figure 8: Process curve of water head of different piezometers located in soil numbered F.
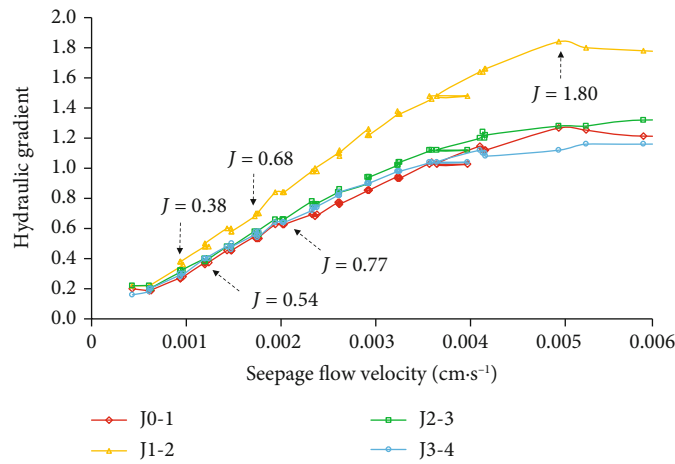

Figure 9: Process curve between hydraulic gradient and seepage flow velocity of different parts in soil numbered F.

allowing both hydraulic pressures and gradients to be observed without diverging or converging flow conditions. Moreover, the necessary conditions for the critical hydraulic gradient to initiate the seepage failure can be assessed. A detailed description of the testing apparatus is given as follows.

The apparatus consists of a water supply device, a sample holder, measuring equipment, and a data collection system. The soil sample is retained in a rigid-walled Plexiglas holder sealed in a porous permeable board attached to a conical, stainless, and influent water supply device. The porous permeable board at the base of the cylinder holds the soil while allowing water to flow gradually into the soil sample. The soil sample holder is a 75.0 cm height and 25.5 cm diameter cylinder-shaped Plexiglas mold with two rows of pore pressure measurement ports located at the sides of the holder, which is designed to precisely measure the hydraulic pressure of seepage flow through the sample at different locations. Piezometric tubes are used to manually measure pore pressure, and sensors connected to the data collection system can automatically measure hydraulic pressure in real time. To better improve the reliability of monitoring data,

measurements are made using 9 pressure sensors (numbered a~i) installed vertically along the side of the apparatus every 5 cm, and 9 piezometric tubes (numbered 0~8) are alternately located on the opposite side every 5 cm, except for the No. 0 tube, which is set in the porous permeable board to measure the upstream water head. The resulting spacing along the vertical allowed the measurements every 2.5 cm to observe minor deformation in each part of the soil in the seepage erosion process. The inside of the sample holder is coated with silicone gel that serves a dual function. First, it provides a frictional interface between the soil samples and the sample holder. Second, since the porous soil sample indents into the silicon, it prevents a preferred seepage path along the edges of the sample that would occur as a consequence of larger interstitial voids caused by a lack of interlocking with the smooth Plexiglas surface.

The hydraulic pressure is flexibly governed by the water tank attached to the screw pole to produce a uniform vertical hydraulic gradient upward through a porous permeable board into the sample. The altitude adjustment is controlled by two nuts arranged on the screw pole that can be fixed on the transmission driver, and the hydraulic pressure can be
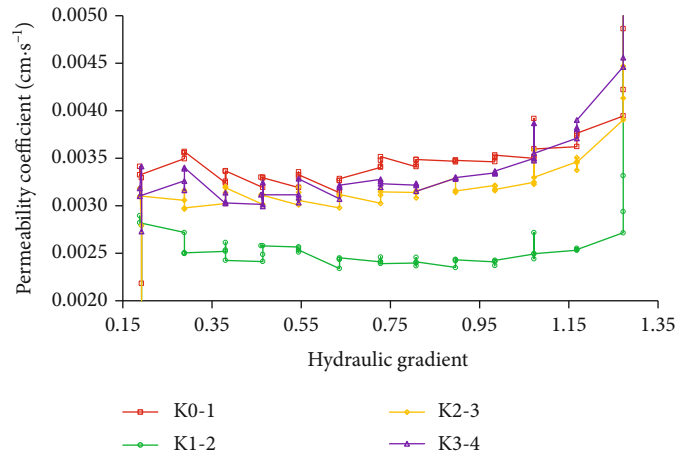
FIGURE 10: Process curve between hydraulic gradient and permeability of different parts in soil numbered F.
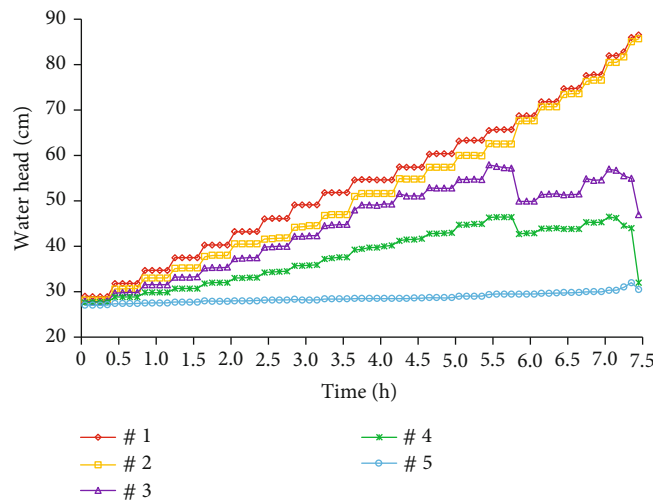

FIGURE 11: Process curve of water head of different piezometers located in soil numbered 1.

slowly regulated. By controlling the upstream head of the water tank and the downstream head of the overflow mouth, the differential head across the sample is steadily increased until initial seepage erosion occurs. At this time, seepage behavior and soil deformation of each part of the porous soil can be observed and recorded.

2.3. Testing Procedure. The testing procedure is outlined as follows:

(1) Control the various factors that may affect seepage failure, including temperature, water content, and soil physical dimension. The constant temperature was kept in the laboratory test. Moreover, soil samples were dried and prepared under the condition of completely saturated water, and the physical dimensions of soil samples were rigidly performed

(2) Different specimen heights were set for testing soils in the sample holder. In particular, the filling height of sandy gravel was typically either 30 cm or 35 cm. If the content of coarse sand was high, the filling height

would be large. Unlike sandy gravel, the filling height requirement for fine-grained sand was 25 cm. All soil samples were filled and compacted to the specified height every 5 cm in layers

(3) Two ways of water supply were used to keep the soil samples gradually saturated. One was to inject water continuously with a slight hydraulic gradient increment of 0.1, but first, ensure that the initial hydraulic gradient was less than 0.1. This test was observed every five minutes until the hydraulic pressure of the sensors varied little or the piezometric tube level was steady. The other was to inject water every 15~30 minutes with a tiny hydraulic gradient increment of 0.05~0.1 to simulate the continuous rise process of the seepage flow

(4) Tests continued before soil samples completely failed when the connected leakage pathway ran through the sample, or soil particles were lifted to float in groups. The quantificational indexes include the hydraulic gradient, the overflow amount, and the
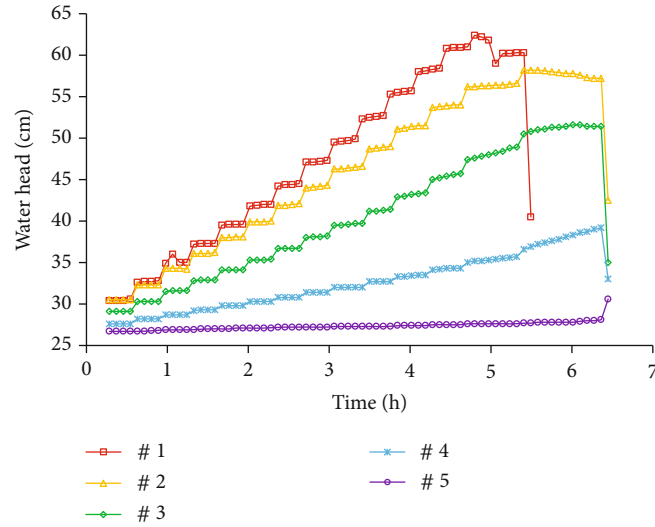
FIGURE 12: Process curve of water head of different piezometers located in soil numbered 2.
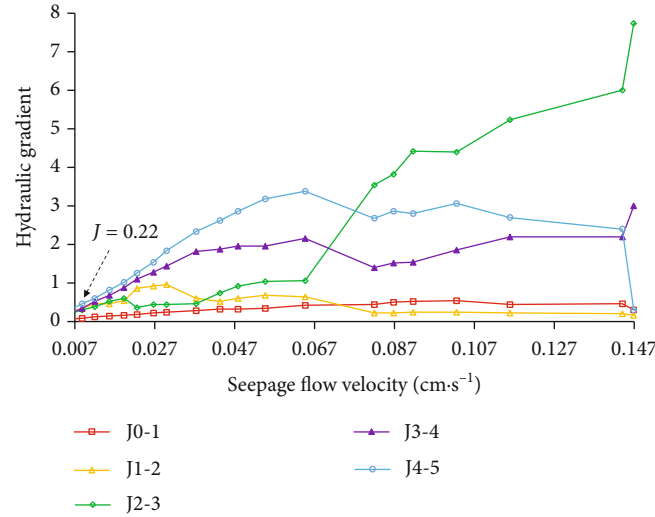

FIGURE 13: Process curve between hydraulic gradient and seepage flow velocity of different parts in soil numbered 1.

permeate coefficient. Tests were not stopped until these indexes increased more than 10 times

(5) Based on the observations of water level in the piezo-metric cubes, hydraulic pressure on the sensors, and turbid degree of the overflow water, the relation curves of the hydraulic gradient to seepage flow velocity (J-v) and permeability coefficient to hydrau-lic gradient (K-J) were established to analyze the spatial-temporal change pattern of the seepage fail-ure process. The turbid degree can be obtained by the mass of wash-out fine fractions per unit volume of overflow water. Considering internal adjustments of fine particles during the seepage failure process, the hydraulic gradient and overflow amount were intensively measured to capture sufficient seepage deformation data. Sands washed from the overflow mouth of the sample holder were sifted to analyze the influenced factor of fine content in the seepage failure process

(6) Note that the seepage flow velocity (v) can be calcu-lated by the overflow amount (Q) and the effective area of the cross-section of the sample holder (nA), namely, $v = Q/nA$. Assuming that the permeability coefficient tends to be a fixed value in a very short time, which is approximately satisfied with Darcy's law, the permeability coefficient at a given time can be deduced by the seepage flow velocity (v) and the hydraulic gradient (J), namely, $K = v/J$

3. Results

3.1. Hydraulic Tests of Seepage Deformation. Seepage defor-mation refers to the phenomenon of the transport of fine particles through the voids of the soil under hydraulic
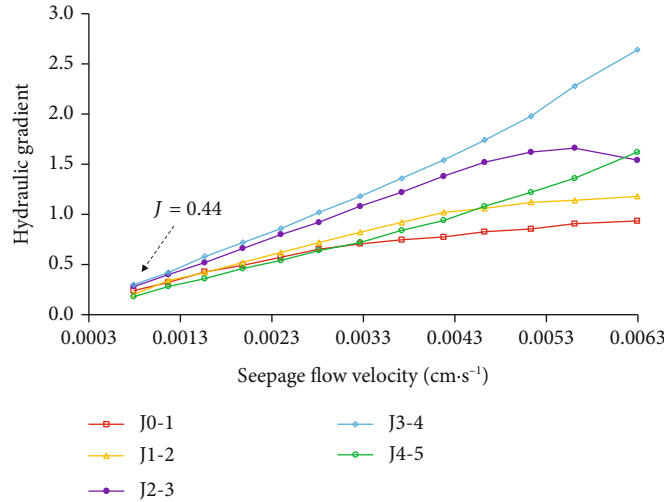
FIGURE 14: Process curve between hydraulic gradient and seepage flow velocity of different parts in soil numbered 2.
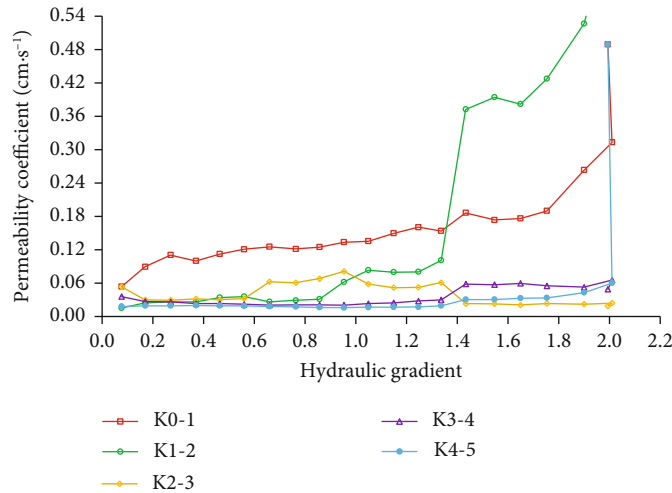

FIGURE 15: Process curve between hydraulic gradient and permeability of different parts in soil numbered 1.

conditions. Hydraulic tests of seepage deformation here mainly show the changes in hydraulic conditions observed by hydraulic gradient, seepage flow velocity, and permeability coefficient, which in turn influence the fluid flow field; hence, the Reynolds number can be deduced using Equation (2) to describe the water flow regime. Take natural soil number C as an example to evaluate sandy gravel seepage behavior of hydraulic gradient (J), seepage flow velocity (v), and permeability coefficient (K). As the hydraulic gradient of the upstream side increases over time, the water levels of the piezometer tubes tend to rise before seepage failure occurs (Figure 5). The process curves (J-v, Figure 6) of the hydraulic gradient to seepage flow velocity were approximately linear when the hydraulic gradient $J < 0.39$, indicating that the permeability coefficient was constant and the soil structure was stable (Figure 7), while the hydraulic gradient $J > 0.39$, seepage deformation first occurred at part 0-1 of the soil sample, and fine particles began to move with little turbid overflow water. When the hydraulic gradient $J = 0.48$,

seepage deformation of internal layers (part 2-3 and part 3-4) appeared. The permeability coefficient continues to increase (Figure 7), accompanied by the phenomena of fines moving in a group, sand boiling from the tube wall, and overflow water becoming turbid. However, as long as the increasing hydraulic gradient $J = 1.40$, the connected leakage pathway from the bottom to the top of the sample was formed with observations of fine particles uplifting together. The water levels of the piezometer tubes suddenly decreased (Figure 5), and the overflow water increased, indicating that the sample soil had completely failed, and the test stopped at the same time.

Take natural soil number F for instance to assess fine-grained sand seepage behavior of hydraulic gradient (J), seepage flow velocity (v), and permeability coefficient (K). As the hydraulic gradient of the upstream side increases over time, the water levels of the piezometer tubes tend to rise before seepage failure occurs (Figure 8). The process curves (J-v, Figure 9) of the hydraulic gradient to seepage flow
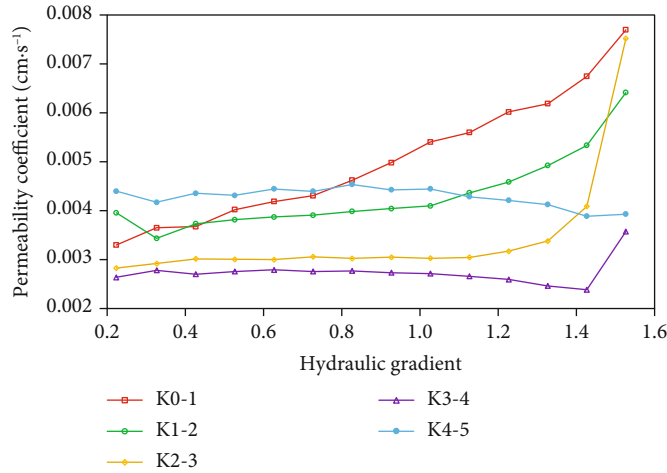
FIGURE 16: Process curve between hydraulic gradient and permeability of different parts in soil numbered 2.
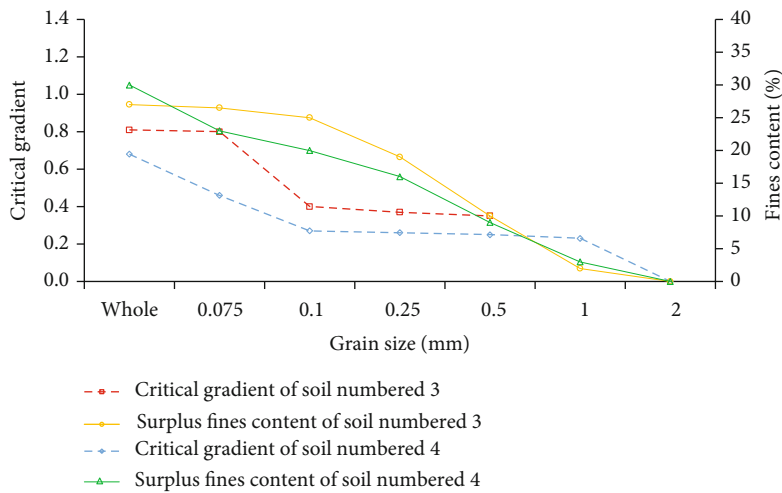

FIGURE 17: Fine content and critical gradient change in the seepage failure process.

velocity were approximately linear when the hydraulic gradient $J < 0.38$, indicating that the permeability coefficient was constant and seepage deformation was not formed. When the hydraulic gradient $J = 0.38$, seepage deformation first appeared in part 3-4 downstream and next appeared in part 2-3 when the hydraulic gradient $J = 0.54$, then in part 0-1 upstream when the hydraulic gradient $J = 0.68$. Eventually, seepage deformation appeared in part 1-2 when the hydraulic gradient $J = 0.77$ and fine particles moved gradually from the connected leakage pathway, and ringlike sands were packed up at the overflow mouth of the soil surface. With the increasing hydraulic gradient $J = 1.80$, the leakage pathway connected upstream to downstream was rapidly developing, accompanied by sands boiling or surface heave.

At the beginning of the test, the permeability coefficient of part 0-1 (K_{0-1}) increased slowly, while the permeability coefficient of part 3-4 (K_{3-4}) increased by jumps under some constraint conditions of overflow exits (Figure 10). During the midterm test, both the permeability coefficient of part 0-1 (K_{0-1}) and part 1-2 (K_{1-2}) increased steadily, while the

permeability coefficient of part 2-3 (K_{2-3}) and part 3-4 (K_{3-4}) decreased by steps because the hydraulic gradient focused temporarily on the downstream as the fine particles moved gradually from upstream into the soil voids of downstream. At the end of the test, the permeability coefficient of part 2-3 (K_{2-3}) and part 3-4 (K_{3-4}) increased rapidly since the hydraulic gradient increased continuously, whereas the permeability coefficient of part 0-1 (K_{0-1}) and part 1-2 (K_{1-2}) altered slightly, indicating that the connected leakage pathway was still developing. Since the hydraulic gradient increased further, all parts of the soil permeability coefficient suddenly increased, indicating that the soil had completely failed.

3.2. Comparative Tests of Seepage Failure. Comparative tests of seepage failure were conducted to show changes in the soil structure by monitoring water levels, overflow amounts, and sand boiling amounts (Figures 11 and 12). Take laboratory-made soil number 1 and number 2 for example to compare the structure changes of sandy gravels in the seepage failure

TABLE 2: Granular soils in the seepage process failure with hydraulic and model-specific parameters.

| Soil type	Soil numbers	Initial gradient	Critical gradient	Failure gradient	Leakage time (min)	Failure time (h)
Natural sandy gravels	A	0.08	0.23	0.29	35	5.5
	B	0.18	0.44	0.51	38	6.0
	C	0.17	0.39	0.48	30	5.0
	D	0.13	0.22	0.32	32	6.5
	E	0.10	0.36	0.43	36	7.0
Natural fine-grained sands	F	0.21	0.68	0.77	92	2.5
	G	0.18	0.57	0.66	80	2.0
	H	0.24	0.51	0.60	85	2.0
	I	0.26	0.82	0.87	78	3.0
Laboratory-made sandy gravels	1	0.15	0.22	0.46	40	6.5
	2	0.19	0.47	0.57	25	6.0
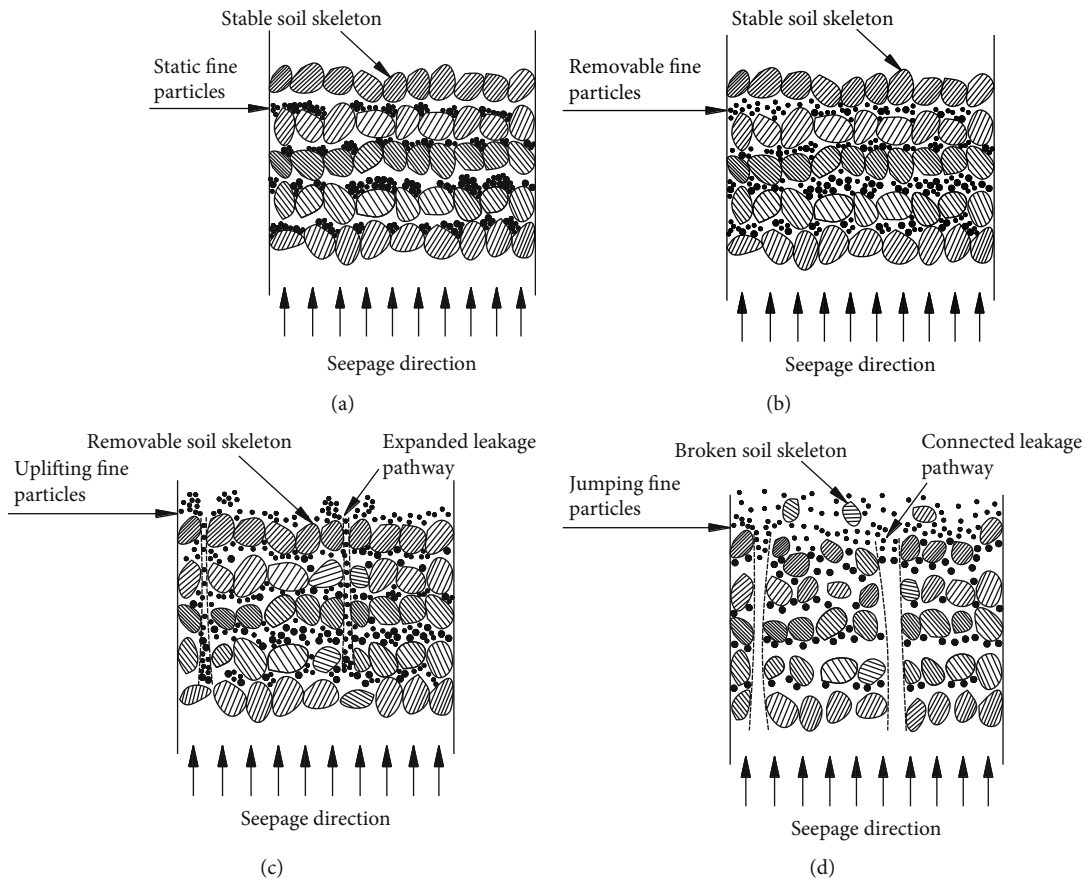
FIGURE 18: Schematic illustration of the entire seepage failure process observed in the experimental modelling: (a) incubation, (b) formation, (c) evolution, and (d) destruction.

process. The hydraulic gradient $J = 0.22$ and fine particles of sample number 1 moved quickly from the leakage pathway and then gradually developed from downstream to upstream (Figure 13). The total failure occurred when the partial deformation increased to two-thirds of the soil, and fine particles were uplifting and floating at this moment. In contrast, the hydraulic gradient $J = 0.44$ in the soil sample numbered

2 and the ring-like sands were piled at the overflow mouth of the soil (Figure 14). As the hydraulic gradient increased further, the deformation ranged from downstream to upstream, thereby rendering the leakage path through the soil with the removal of fine particles in groups. Meanwhile, the soil surface heaved and then became completely unstable. The permeability coefficient has doubled with the possible reason for
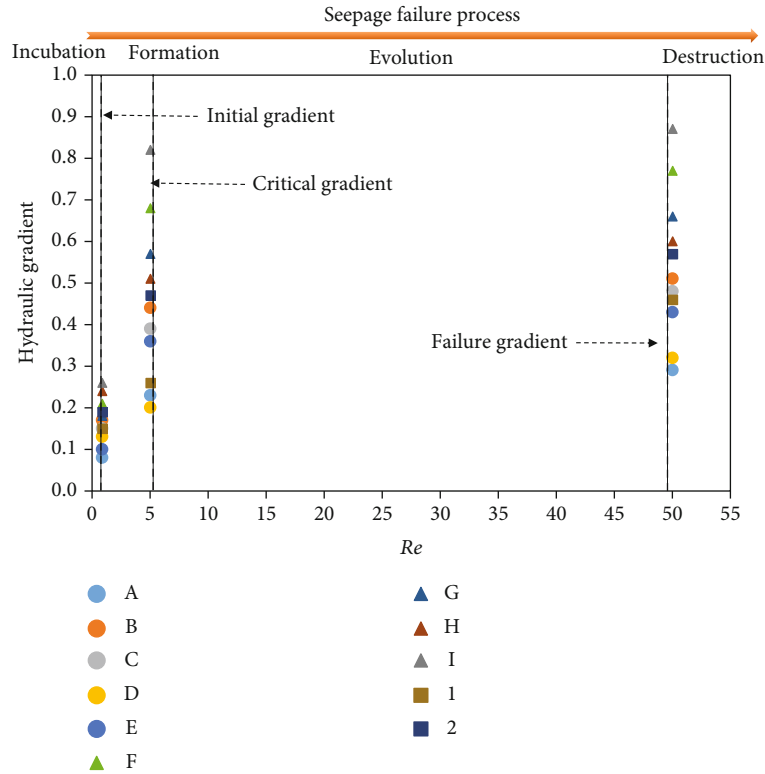
FIGURE 19: Various samples of failure process division with the Reynolds number and hydraulic gradient.

the compactness and fine content of the soil (Figures 15 and 16).

3.3. *Particle Flow Tests of Gapped Grading Soil.* To shed light on the essential factors that affect the development of the seepage failure process, different sizes of soil particles (numbered 3 and 4) were sifted out and prepared to be gapped-grading samples. Long-term tests, including seven groups of soil tests (i.e., complete test, <0.075 mm particles absent test, <0.10 mm particles absent test, <0.25 mm particles absent test, <0.50 mm particles absent test, <1 mm particles absent test, and <2 mm particles absent test), were performed to analyze different fine contents that affect the seepage failure process (Figure 17).

When soil number 3 was complete, the fine content was 27%, and the hydraulic gradient was 0.82. Similarly, the fine content is 26% with the absence of grain size < 0.075 mm, and the hydraulic gradient is 0.80. The phenomena of floating particles and heaving surfaces were observed in the above two tests. However, the fine content is 24% with the absence of grain size < 0.10 mm, and the hydraulic gradient suddenly dropped to 0.40. At the same time, fine particles moved gradually from the leakage pathway with turbid overflow water, but the soil skeleton was unbroken. The fine content is 19% with the absence of grain size < 0.25 mm, and the hydraulic gradient slowly decreased to 0.37. In the absence of 0.50 mm grain size, the fine content was only 10%, and the hydraulic gradient dropped to 0.33, accompanied by piping deformation. The results show that sample number 3 of the soil skeleton was still unbroken when the connected

pathway forms. Similarly, for sample number 4, the critical gradient is 0.58 without the absence of gains, accompanied by flowing soil deformation. As grains of <0.075 mm size were removed, the fine content was 23%, and the critical gradient decreased to 0.46 with the observation of piping deformation. When all the fines in sample number 4 were removed, the permeability coefficient increased highly, even if the hydraulic gradient increased to 0.70, but the soil skeleton was still unbroken.

4. Discussion

4.1. *Seepage Failure Process Division.* As described in the results, seepage deformation develops from the external part to the internal part of the soil samples, indicating that the hydraulic gradient decreases in the deformation parts and the permeability coefficient increases. Since the hydraulic gradient progressively increases, soil deformation has been continuously expanded. As a result, soil failure occurs when the hydraulic gradient increases to a certain value. Both sandy gravels and fine-grained sands share some similarities but differ in time in the seepage failure process, as shown in Table 2. The important parameters in Table 2 are explained as follows. Initial gradient means that seepage begins to flow after overcoming the resistance of film water with the appearance of small visible deformation, which can be obtained by J-v process curves on the vertical coordinate when the seepage flow velocity $v = 0$. Critical gradient means that the hydraulic gradient reaches the critical state; that is, seepage force is the equivalent of soil buoyant unit weight,

TABLE 3: Phase division in the seepage failure process based on the Reynolds number.

| Soil number	Linear change process		Nonlinear change process	
	Incubation	Formation	Evolution	Destruction
A	Re < 0.62	0.62 ≤ Re ≤ 5.13	5.13 < Re ≤ 51.34	51.34 < Re
B	Re < 0.86	0.86 ≤ Re ≤ 4.80	4.80 < Re ≤ 53.28	53.28 < Re
C	Re < 0.76	0.76 ≤ Re ≤ 4.95	4.95 < Re ≤ 52.57	52.57 < Re
D	Re < 0.72	0.72 ≤ Re ≤ 5.10	5.10 < Re ≤ 49.98	49.98 < Re
E	Re < 0.68	0.68 ≤ Re ≤ 5.02	5.02 < Re ≤ 51.23	51.23 < Re
F	Re < 0.62	0.62 ≤ Re ≤ 5.13	5.13 < Re ≤ 50.85	50.85 < Re
G	Re < 0.77	0.77 ≤ Re ≤ 4.85	4.85 < Re ≤ 49.55	49.55 < Re
H	Re < 0.78	0.78 ≤ Re ≤ 5.08	5.08 < Re ≤ 51.21	51.21 < Re
I	Re < 0.85	0.85 ≤ Re ≤ 5.11	5.11 < Re ≤ 49.69	49.69 < Re
1	Re < 0.87	0.87 ≤ Re ≤ 5.20	5.23 < Re ≤ 49.88	49.88 < Re
2	Re < 0.79	0.79 ≤ Re ≤ 5.13	5.13 < Re ≤ 50.70	50.70 < Re
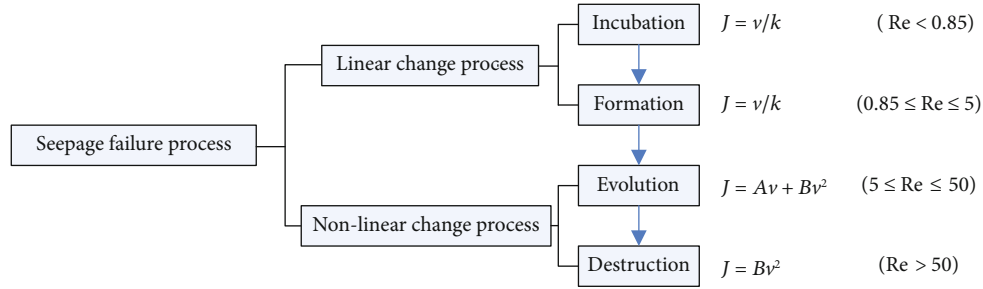
FIGURE 20: Piecewise function of seepage failure process division with the Reynolds number.

and soil deformation expands to the whole soil with the connected leakage pathway from top to bottom. The failure gradient represents the hydraulic gradient that stops the test when the overflow amount suddenly increases with a permeability coefficient of more than ten times. Leakage time represents the time that the leakage pathway runs through the soil sample, but the soil skeleton is still unbroken. Failure time means that complete deformation appears and the soil skeleton is broken. According to the analysis of Table 2, leakage time in sandy gravels is relatively short (about 25 min-40 min), but failure time is fairly long (about 5 h-7 h). Leakage time in fine-grained sands is much longer (about 78 min-92 min), but failure time is reasonably short (about 2 h-3 h), which means fine-grained sands are not easy to initiate seepage deformation. Once the leakage path is formed, the soil structure appears unstable. Despite the removal of fine particles from the leakage path, the sandy gravels still maintain stability because the increasing seepage gradient is not enough to break the soil skeleton. According to the time sequence of the seepage process, the hydraulic gradient focuses on the exit face first, resulting in the start and migration of fine particles, which drives the development of seepage deformation upstream. Imposed by the seepage force, different parts of the soil deformation appear in succession with an increase in the hydraulic gradient.

As observed in the tests, the entire process of seepage failure can be qualitatively divided into four phases: (i) incubation, (ii) formation, (iii) evolution, and (iv) destruction (Figure 18). There is a difference between hydraulic and mechanical characteristics in different phases of the seepage failure process. First, in the incubation phase, soil particles are not started without any soil deformation at a small hydraulic gradient. Next, in the formation phase, the surface grains are slowly loosened, so that soil deformation is gradually formed when reaching the initial hydraulic gradient. At this point, both the seepage force and the viscous shear force imposed on the soil grains reach the magnitude of the retaining forces at the exit face. However, the migration of soil particles increases the size of the surrounding interstitial voids, resulting in slight deformation, but soil skeletons are still stable and deformations are not apparent in this phase. Then, in the evolution phase, as the hydraulic gradient is again increased to the critical gradient, the surface grains move rapidly until the void ratio reaches the maximum. The increasing hydraulic gradient reduces the downward force of the upper grains on the next layer of underlying grains, resulting in a loose zone. This evolution process is not stopped until the loosened zone expands rapidly in thickness and the exit face of the sample progressively heaves. Since the hydraulic gradient constantly increases, soil deformation gradually develops to approximately two-

TABLE 4: Experimental results of different fine contents in sandy gravels.

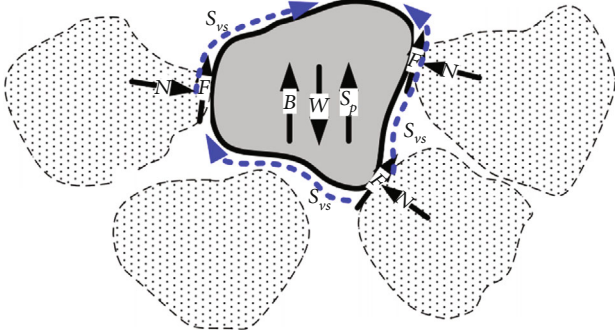| Soil number	Fine content (%)	Permeability coefficient (cm·s^{-1})	Initial gradient	Critical gradient	Failure gradient	Leakage time (min)
1	18	3.35×10^{-2}	0.15	0.22	0.46	40
C	27	1.10×10^{-2}	0.17	0.39	0.48	30
2	30	4.00×10^{-3}	0.19	0.47	0.57	25

FIGURE 21: Schematic illustration of various forces acting on a soil particle at the exit face of soil sample (adapted from [11]).

thirds of the seepage path length. Finally, in the destruction phase, sand boil or total heave appears at the failure gradient, accompanied by large interstitial voids on the near surface of the soil sample. A preferential seepage flow pathway is gradually formed, which is similar to a relief well, allowing water to escape from the sample. Since the water flows continuously, the preferential pathway pressure is finally relieved. The fine particle migration increases the permeability coefficient of the soil surrounding the preferential pathway. As a result, the pathway is expanded to provide drainage for the inside of the sample. As long as the heaved zone remains effectively on top of the soil sample, the equilibrium process can be kept as the remaining downward force of the upper grains continues to impose on the lower grains. Nevertheless, sloughing of the heaving mound will occur when the sides of the heaving mound exceed a steady inclination, which removes the overburden of the loosened zone and prevents equilibrium from being achieved. At this time, the soil suddenly fails.

Since the fine particles gradually transport from the expanding leakage pathway, the water flow regime changes accordingly, which can be quantitatively measured by the Reynolds number. The average flow velocity can be determined by the cross-section of the overflow water. The average flow velocity of the cross-section is an imaginary value based on the assumption of the same flow velocity of every point of the efficient cross-section; therefore, the volume of the overflow water is approximately equal to the actual value. Furthermore, the important parameters, such as water density ($1 \, \mathrm{g/cm^3}$), water viscosity ($0.84E - 3 \, \mathrm{Pa \cdot s}$) at ordinary temperature, and characteristic soil particle size (d_{50}), can be also easily obtained; hence, the Reynolds number can be calculated using Equation (2). Despite a difference in the hydraulic gradient, the Reynolds numbers of various soils present a similar feature (Figure 19). According to the distri-

bution characteristics of the Reynolds number, seepage failure can generally be divided into linear change process and nonlinear change process, as shown in Table 3 and Figure 20. When Re < 0.85, the seepage section forms without particle removal in the incubation phase. When $0.85 \leq$ Re ≤ 5, fine particles are slowly adjusted at the initial gradient and a leakage pathway is gradually formed in the formation phase. In the above two phases, the viscous drag force holds a dominant position, so the relationship between hydraulic gradient and seepage velocity presents approximately linearity, which conforms to Darcy's law. While $5 <$ Re ≤ 50, the leakage pathway develops rapidly in the phase of evolution at the critical gradient, bringing major changes in seepage velocity. Consequently, the laminar flow gradually changes into turbulent motion. When $50 < $ Re, seepage velocity changes dramatically in the destruction phase at the failure gradient due to the turbulent flow. At this point, the hydraulic gradient and the seepage velocity are nonlinearly related; meanwhile, inertial force plays a great role, and the quadratic equation can be applied to describe these two phases (Figure 20).

4.2. Seepage Failure Process Mechanism. Based on the quantitative description of the seepage failure process, the seepage failure mechanism needs to be further clarified by comparing the results of various hydraulic tests. For example, given the seepage deformation results of soil numbered 1, numbered C, and numbered 2, different fine contents of sandy gravels are compared to reveal the factors affecting the seepage failure process (in Table 4). Note that fine particles herein refer to soil particles with diameter < 2 mm and not <0.075 mm, as generally assumed in the geomechanics community. Results show that the higher the fine content, the smaller the permeability coefficient, the larger the hydraulic gradient, and the shorter the leakage time. Sandy gravels composed of low fine content easily produce deformation, but it takes a long time to form the run-through pathway. By comparison, sandy gravels with high fine contents are difficult to cause seepage deformation even if the hydraulic gradient increases to a large magnitude. Once the hydraulic gradient is increased to affect the soil skeleton, the deformation develops rapidly with the expanding seepage pathway. Obviously, fine content and uniformity coefficient are key factors influencing each phase of the seepage failure process.

Despite inherent influence factors of fine content and uniformity, the forces imposed on the darker-shaded sand grain are required to clarify the seepage failure process mechanism in Figure 21, which shows a grain at the exit face of a test sample. As a vertical hydraulic gradient acts on the sample, the forces imposed on the grain include (1)

the weight of the grain, W, (2) the buoyant force, B, (3) the seepage force resulting from the differential hydraulic pressures between the top and bottom of grain, S_p, (4) the viscous shear forces from the seeping water S_v, and (5) the normal, N, and shear, F, forces at intergranular contacts. Note that the seepage force is a body force imposed on the soil skeleton by seepage flow, including the thrust force and the drag force, which is similar to S_p and S_v. The seepage force is essentially caused by the hydraulic gradient across the grain. If water flow is upward, as presented in this paper, the seepage force is proportional to the hydraulic gradient acting across the grain; that is, the seepage force is directly proportional to differential hydraulic pressures, but it is inversely proportional to the length of the seeping path. Specifically, at the very top of the sample where the grain is on the surface, the grains can be individually removed without any component of normal and frictional forces acting on them before the migration occurs. Given the state of incipient movement, the surface grains begin to transport with an increasing hydraulic gradient. The loosened soil has both more void space and larger interstitial voids than before, allowing seeping water to flow slower through the mass and less shear stress on the grains. In particular, the seepage force can be understood as a function of the seepage flow velocity and the interstitial void size. Since it seeps through a void, the water flows at a maximum velocity in the center of the void but decreases to approximately zero adjacent to the void. Based on Navier-Stokes equations, the magnitude of the viscous shear acting on the grain gets increased not only as the average velocity through the void increases but also as the distance from the maximum velocity to the grain surface decreases. As the size of the void increases, the velocity of the seeping water decreases, and the shear transfer from the water to the grain decreases due to the greater distance to the maximum flow velocity.

From the discussion above, it is obvious that the seepage force acting on the soil motivates the migration of grains, while gravity and friction resist the movement of the grain in the vertical seepage force. Under the same uniformity condition, the larger the size of the sand, the greater the gravity, and the stronger the critical stress. More specifically, for sandy gravels with uniformity coefficient $Cu > 5$, the friction of the surrounding grains may play a resistant role if the soil is compacted with a high fine content. However, the gravity associated with grain size controls the resistance of particle movement if the soil is loose with a low fine content. If the fine content exceeds 25%, the hydraulic gradient is large enough to result in particle floating and soil heaving. But if the fine content is less than 25%, the smaller the grain size and hydraulic gradient, the more easily piping failure may occur. For fine-grained sands with the coefficient of uniformity $Cu \leq 5$, the friction acts on particles with a major resistance of particle start-up. If particles are well graded, the seepage failure observations ultimately present particle floating and soil heaving, whereby the hydraulic gradient reaches a large magnitude. In contrast, if the soil is loose, nonuniform, or poorly graded, piping failure is more likely to occur at a small hydraulic gradient.

5. Conclusions

In this study, a series of hydraulic tests, including seepage deformation tests, comparative tests, and particle flow tests, were performed to clarify the evolution mechanisms of the seepage failure process in granular soils. The main conclusions are as follows:

(1) The description method of the seepage failure process was proposed to quantitatively distinguish the fluid regime changes based on the distribution characteristics of the Reynolds number. Four phases of the seepage failure process were identified by the Reynolds number in sandy gravels and fine-grained sands: (i) incubation (Re < 0.85), (ii) formation (0.85 ≤ Re ≤ 5), (iii) evolution (5 < Re ≤ 50), and (iv) destruction (50 < Re)

(2) Different mechanisms of particle migration and mechanical behavior were clarified by analysis of experimental results. In the phases of incubation and formation, the relationship between hydraulic gradient and seepage velocity is approximately linearity, indicating that the viscous drag force holds a dominant position that conforms to Darcy's law. In the phases of evolution and destruction, the hydraulic gradient and the seepage velocity are nonlinearly related. The inertial force plays a leading role, and the quadratic equation can be applied to describe the gradual transition from laminar flow to turbulent motion

(3) Fine content and uniformity coefficient are key factors affecting the seepage failure process, while seepage force is the underlying cause of particle migration in the seepage failure process. Piping failure is more likely to be triggered in sandy gravels with a uniformity coefficient greater than 5 and fine content less than 25%. Seepage force drives some fine particles to escape from the seepage pathway, but the soil skeleton still remains stable for a long time before seepage failure occurs. Heaving failure always occurs in fine-grained sands with a uniformity coefficient less than 5 and fine content higher than 25%. Seepage force motivates all the loosened particles to flow in groups at a large critical hydraulic gradient

The observations of the hydraulic tests provide a deeper understanding of every phase of the seepage failure process. The methods and results may be of interest to hydrologists, environmental scientists, and water engineers who focus on seepage failure in granular soils. This paper is limited by hydraulic tests to sandy gravels and fine-grained sands. Further research with a wider variety of soil types and more advanced visualization technology is encouraged to provide more insights into the mechanisms of the seepage failure process.

Symbols

a: Constant (-)
B: Buoyant force acting on a grain of soil (M)
β: Non-Darcy coefficient (L^{-1})
C_u: Uniformity coefficient (-)
d: Characteristic length (L)
d_{10}: Size of particle corresponding to 10% passing of coarse fraction (L)
d_{50}: Size of particle corresponding to 50% passing of coarse fraction (L)
J: Hydraulic gradient (-)
K: Permeability coefficient (LT^{-1})
k_d: Darcy permeability (LT^{-1})
k_f: Forchheimer permeability (LT^{-1})
L: Length between the inlet and outlet (L)
m: Variable parameter subjected to fluid regime change (-)
n: Porosity (-)
$\triangle p$: Fluid pressure (ML^{-2})
ρ: The fluid density (ML^{-3})
ρ_d: Soil dry density (ML^{-3})
μ: Fluid viscosity (MLT^{-1})
v: Flow velocity (LT^{-1})
W: Weight (M)
Re: Reynolds number (-)
N: Normal forces (ML^{-2})
S_p: Seepage force (ML^{-2})
S_{vs}: Viscous shear force (ML^{-2}).

Data Availability

The data used to support the findings of this study are available from the corresponding author upon request.

Conflicts of Interest

The authors declare that there is no conflict of interests regarding the publication of this article.

Acknowledgments

References

[1] C. F. Wan and R. Fell, "Investigation of rate of erosion of soils in embankment dams," *Journal of Geotechnical and Geoenvironmental Engineering*, vol. 130, no. 4, pp. 373–380, 2004.

[2] M. Foster, R. Fell, and M. Spannagel, "The statistics of embankment dam failures and accidents," *Canadian Geotechnical Journal*, vol. 37, no. 5, pp. 1000–1024, 2000.

[3] Y. Wang, X. B. Duan, Y. C. Gu, and S. J. Wang, "Fractal characteristics of the seepage erosion process in porous soil," *Geofluids*, vol. 2022, Article ID 3383773, 12 pages, 2022.

[4] T. L. Wahl, K. W. Frizell, and H. T. Falvey, "Uplift pressures below spillway chute slabs at unvented open offset joints," *Journal of Hydraulic Engineering*, vol. 145, no. 11, article 04019039, 2019.

[5] D. M. Gu, D. Huang, H. L. Liu, W. G. Zhang, and X. C. Gao, "A DEM-based approach for modeling the evolution process of seepage-induced erosion in clayey sand," *Acta Geotechnica*, vol. 14, no. 6, pp. 1629–1641, 2019.

[6] N. J. Jiang, K. Soga, and M. Kuo, "Microbially induced carbonate precipitation for seepage-induced internal erosion control in sand-clay mixtures," *Journal of Geotechnical and Geoenvironmental Engineering*, vol. 143, no. 3, article 04016100, 2016.

[7] L. Ke and A. Takahashi, "Experimental investigations on suffusion characteristics and its mechanical consequences on saturated cohesionless soil," *Soils and Foundations*, vol. 54, no. 4, pp. 713–730, 2014.

[8] K. S. Richards and K. R. Reddy, "Experimental investigation of initiation of backward erosion piping in soils," *Geotechnique*, vol. 62, no. 10, pp. 933–942, 2012.

[9] F. Bendahmane, D. Marot, and A. Alexis, "Experimental parametric study of suffusion and backward erosion," *Journal of Geotechnical and Geoenvironmental Engineering*, vol. 134, no. 1, pp. 57–67, 2008.

[10] C. D. Nguyen, N. Benahmed, E. Ando, L. Sibille, and P. Philippe, "Experimental investigation of microstructural changes in soils eroded by suffusion using X-ray tomography," *Acta Geotechnica*, vol. 14, no. 3, pp. 749–765, 2019.

[11] P. Sige and D. R. John, "Measuring critical gradients for soil loosening and initiation of backward erosion-piping mechanism," *Journal of Geotechnical and Geoenvironmental Engineering*, vol. 146, no. 8, article 04020069, 2020.

[12] D. Ma, H. Y. Duan, J. X. Zhang, X. J. Feng, and Y. L. Huang, "Experimental investigation of creep-erosion coupling mechanical properties of water inrush hazards in fault fracture rock masses," *Chinese Journal of Rock Mechanics and Engineering*, vol. 40, no. 9, pp. 1751–1763, 2021.

[13] A. Wörman and R. Olafsdottir, "Erosion in a granular medium interface," *Journal of Hydraulic Research*, vol. 30, no. 5, pp. 639–655, 1992.

[14] H. J. Kim, J. M. Park, and J. H. Shin, "Flow behaviour and piping potential at the soil-structure interface," *Geotechnique*, vol. 69, no. 1, pp. 79–84, 2019.

[15] A. S. Yusuf, E. Mohamed, M. H. Chaudhry, and I. Jasim, "Experimental study on the piping erosion process in earthen embankments," *Journal of Hydraulic Engineering*, vol. 141, no. 7, article 04015012, 2015.

[16] L. L. Zeng, Y. Q. Cai, Y. J. Cui, and Z. S. Hong, "Hydraulic conductivity of reconstituted clays based on intrinsic compression," *Geotechnique*, vol. 70, no. 3, pp. 268–275, 2020.

[17] X. D. Ni, Y. L. Niu, Y. Wang, and K. Yu, "Non-Darcy flow experiments of water seepage through rough-walled rock fractures," *Geofluids*, vol. 2018, Article ID 8541421, 12 pages, 2018.

[18] C. Bordier and D. Zimmer, "Drainage equations and non-Darcian modelling in coarse porous media or geosynthetic materials," *Journal of Hydrology*, vol. 228, no. 3-4, pp. 174–187, 2000.

[19] Y. Li, Z. Zhou, C. Zhuang, Y. Huang, and J. Wang, "Non-Darcian effect on a variable-rate pumping test in a confined aquifer," *Journal of Hydrology*, vol. 28, no. 8, pp. 2853–2863, 2020.

[20] Y. Wang, S. J. Wang, X. B. Duan, Y. C. Gu, Q. Pang, and C. Yang, "Physical modelling of initial seepage failure process," *International Journal of Physical Modelling in Geotechnics*, vol. 15, no. 4, pp. 1–9, 2015.

[21] A. Otaru and A. Kennedy, "Investigation of the pressure drop across packed beds of spherical beads: comparison of empirical models with pore-level computational fluid dynamics simulations," *Journal of Fluids Engineering*, vol. 141, no. 7, article 071305, 2019.

[22] D. Ma, H. Y. Duan, X. B. Li, Z. H. Li, Z. Zhou, and T. B. Li, "Effects of seepage-induced erosion on nonlinear hydraulic properties of broken red sandstones," *Tunnelling and Underground Space Technology*, vol. 91, no. 9, article 102993, 2019.

[23] I. Haghighi, C. Chevalier, M. Duc, S. Guedon, and P. Reiffsteck, "Improvement of hole erosion test and results on reference soils," *Journal of Geotechnical and Geoenvironmental Engineering*, vol. 139, no. 2, pp. 330–339, 2013.

[24] H. Tao and J. Tao, "Quantitative analysis of piping erosion micro-mechanisms with coupled CFD and DEM method," *Acta Geotechnica*, vol. 12, no. 3, pp. 573–592, 2017.

[25] D. Ma, W. T. Hou, J. X. Zhang, J. J. Wang, Z. H. Li, and D. Feng, "Radial seepage-axial stress characteristics of hollow rock sample and seepage mutation mechanism of roadway surrounding rock," *Journal of China Coal Society*, vol. 21, pp. 1–18, 2022.

[26] D. Ma, H. Y. Duan, W. T. Liu, X. T. Ma, and M. Tao, "Water-sediment two-phase flow inrush hazard in rock fractures of overburden strata during coal mining," *Mine Water and the Environment*, vol. 39, no. 2, pp. 308–319, 2020.

[27] S. F. Mandie and D. R. John, "Laboratory modeling of the mechanisms of piping erosion initiation," *Journal of Geotechnical and Geoenvironmental Engineering*, vol. 140, no. 6, article 04014017, 2014.

[28] F. Mercier, S. Bonelli, F. Golay, F. Anselmet, P. Philippe, and R. Borghi, "Numerical modelling of concentrated leak erosion during hole erosion tests," *Acta Geotechnica*, vol. 10, no. 3, pp. 319–332, 2015.

[29] K. S. Richards and K. R. Reddy, "Critical appraisal of piping phenomena in earth dams," *Bulletin of Engineering Geology and the Environment*, vol. 66, no. 4, pp. 381–402, 2007.

[30] K. L. Tian, A. Q. Yang, K. Y. Nie, H. L. Zhang, J. Xu, and X. D. Wang, "Experimental study of steady seepage in unsaturated loess soil," *Acta Geotechnica*, vol. 15, no. 9, pp. 2681–2689, 2020.

[31] F. Zhang, M. Li, M. Peng, C. Chen, and L. Zhang, "Three-dimensional DEM modeling of the stress-strain behavior for the gap-graded soils subjected to internal erosion," *Acta Geotechnica*, vol. 14, no. 2, pp. 487–503, 2019.

[32] Y. Wang, Y. C. Gu, S. J. Wang, and X. B. Duan, "Permeability coefficient investigation based on fractal characteristics of porous media soil," *Hydro-Science and Engineering*, vol. 2022, no. 3, pp. 50–58, 2022.